ROLE OF TEMPERATURE ON RAMAN SPECTROSCOPY OF MOS_2 MONOLAYER SYNTHESIZED BY CHEMICAL VAPOUR DEPOSITION (CVD)

DISSERTATION

SUBMITTED TO
DEPARTMENT OF PHYSICS
SCHOOL OF PHYSICAL SCIENCES
DOON UNIVERSITY, DEHRADUN

IN PARTIAL FULFILLMENT OF THE REQUIREMENTS
FOR THE AWARD OF THE DEGREE OF

MASTER IN PHYSICS

SUBMITTED
BY
BHUVAN SINGH BHANDARI
20PH-68

DEPARTMENT OF PHYSICS
SCHOOL OF PHYSICAL SCIENCES
DOON UNIVERSITY, DEHRADUN UTTARAKHAND (INDIA)
2022

Declaration

I declare that the work presented in the Dissertation entitled **"Role of temperature on Raman Spectroscopy of MoS_2 monolayer synthesized by chemical vapour deposition method (CVD)"** being submitted to the Department of Physics, School of Physical Scences, Doon University, Dehradun for the award of Master in Physics is my original research work.

The Dissertation embodies the results of investigations, observations, and experiments carried out by me. I have neither plagiarized any part of the dissertation nor have submitted same work for the award of any other degree/diploma anywhere.

…….....

Bhuvan Singh Bhandari

20PH-68

Date:___/ 08 / 2022

Certificate

This is to certify that Dissertation entitled **"Role of temperature on Raman Spectroscopy of MoS_2 monolayer synthesized by chemical vapour deposition method (CVD)"** submitted by Bhuvan Singh Bhandari has been done under my supervision. It is also certified that the work in this Dissertation embodies original research and hard work of the candidate. The assistance and support received during the course of investigation and all the sources of literature have been fully acknowledged.

Supervisor/Guide

Dr. Himani Sharma

Assistant Professor

Department of Physics

School of Physical Sciences

Doon University

Head, Department of Physics

Dr. Himani Sharma

School of Physical Sciences

Doon University

Acknowledgment

I express my deep gratitude to my project supervisor Dr. Himani Sharma ma'am for providing me with the opportunity to work under her supervision and encourage, motivated, supported and provided me such an informative environment during my project work. Her full support, constant assistance and guidance helped me and encouraged me tackling the obstacles and led to develop a positive attitude and appreciation for the subject.

I would like to express my deep gratitude to research scholars Mr. Saurabh Rawat sir and Dr. Priyanka Bamola ma'am, for their constant support and assistance throughout the project. They worked very hard throughout in introducing us to the lab equipment, apparatuses, machines and their workings. Their constant push and assistance in understanding the concepts and mechanisms had only led to the successful completion of project on time. They developed a good interaction with me along with everybody else and appreciated to ask doubts and helped clearing the doubts regarding any operations of machines and working of required computer applications. They constantly monitored our work and insisted to maintain discipline, cleanliness, and take necessary precaution while operating equipment. Also I express my deep gratitude to Dr. Rajesh sir for providing me the data of Raman Spectroscopy.

Secondly, I would like to express my sincere appreciation to my lab-mates and colleagues Ms. Monika Bisht, Ms. Shreya Negi, Mr. Abhinav Bhatt, Ms. Deepali Aswal, and Ms. Stuti Dhapola for their cooperation and creating a healthy atmosphere during the course of project. Their collective problem discussing attitude and assistance had been quite helpful.

Bhuvan Singh Bhandari

20PH-68

Abstract

The two-dimensional (2D) atomically thin transition metal dichalgogenides (TMDCs) materials like grapheme, graphene MoS_2, WS_2, $MoSe_2$ and others, have attracted interest because they offer useful features for optoelectronics and nanoelectronics device applications. Graphene is a fundamental two-dimensional sheet of carbon atoms with exceptional mechanical, thermal, optical and electronic properties that are absent in its bulk counterparts. But graphene does not have an intrinsic band gap which makes it unlikely to be used in semiconductors.

MoS_2, a semiconductor material just like graphene, has sparked interest around the world due to its unique features, including as changeable bandgap, high carrier mobility, ultra-thin thickness, and significant absorption at visible frequencies.

The ability to shift the bandgap from monolayer to bulk has an impact on numerous properties such as electrical, optical, chemical, magnetic, and mechanical properties, indicating its potential use in various nanoelectronics and optoelectronic devices. However, a device's performance is entirely dependent on the structural characteristics and thermal conductivity of the materials, which are affected by factors like as pressure and temperature. The monolayer of MoS_2 has a direct band gap of 1.8 eV, while the bulk MoS_2 is a semiconductor with an indirect band gap of 1.2 eV.

Following a literature review and analysis of past work on molybdenum sulphide synthesis, we determined that chemical vapour deposition (CVD) was the optimum option due to adjustable size and layer numbers.

In this research work we used the chemical vapour deposition approach to make MoS_2 monolayer, changing the temperatures of the zones, deposition/growth duration, rate of flow of inert carrier gas, precursor ratio, and other parameters in a controlled environment. MoS_2 is produced and placed on SiO_2 substrates and we examined the temperature dependent Raman Spectroscopy of CVD synthesized monolayer MoS_2 and its structural features were examined by Raman Spectroscopy at different temperatures (273k to 573k).

The composition, structure and morphology is studied using optical microscopy, Scanning electron microscopy(SEM), Raman Spectroscopy, X-ray diffraction(XRD) and X-ray photoelectron spectroscopy(XPS).

Contents

List of Tables

List of Figures

Chapter 1

Introduction

1.1 Background

The demand for (2D) materials like graphene with exceptional electrical characteristics has grown recently. The first 2D material to be created was graphene, which introduced the idea of materials only one atom thick. The fact that the valence band and conduction band touch makes it semi-metal. Graphene cannot be used in semiconductor materials since it has a zero band gap. With similar qualities to graphene and addressing the drawbacks of the zero bandgap, 2D TMDs were discovered to be the ideal substitute for graphene.

The band gap features of 2D TMDs, semiconductor materials with distinctive electrical, mechanical, and optical properties, appeared to be extremely promising for usage in next-generation semiconductor devices. Because of its fascinating electrical and optical features, MoS_2 is a typical TMDC that is generating significant scientific interest.

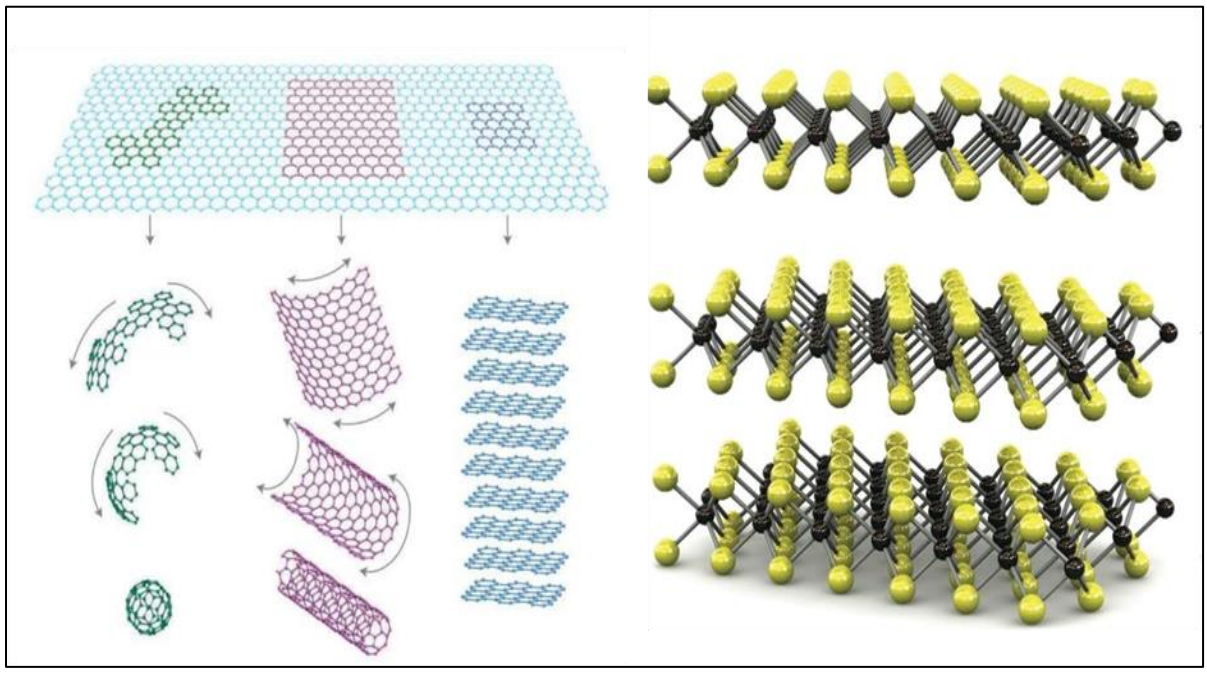

Figure 1.1 (a)Graphene is a 2D material for carbon building materials of all other dimensions SOURCE:(PDF) Formulation of 2D Graphene Deformation Based on Chiral-Tube Base Vectors. (b) Schematic of atomic structure of MoS_2. SOURCE: By Xin Tao ResearchGate. SOURCE: (PDF) Formulation of 2D Graphene Deformation Based on Chiral-Tube Base Vectors. SOURCE: By Xin Tao ResearchGate.

1.2 Transition Metal Dichalcogenides (TMDCs)

TMDCs are atomically thin semiconductors of the type MX_2 where M is a transition metal atom and X is a chalcogen atom. A layer of M atoms is sandwiched between two layers of X atoms. The metal can have either trigonal prismatic or octahedral coordination[1].

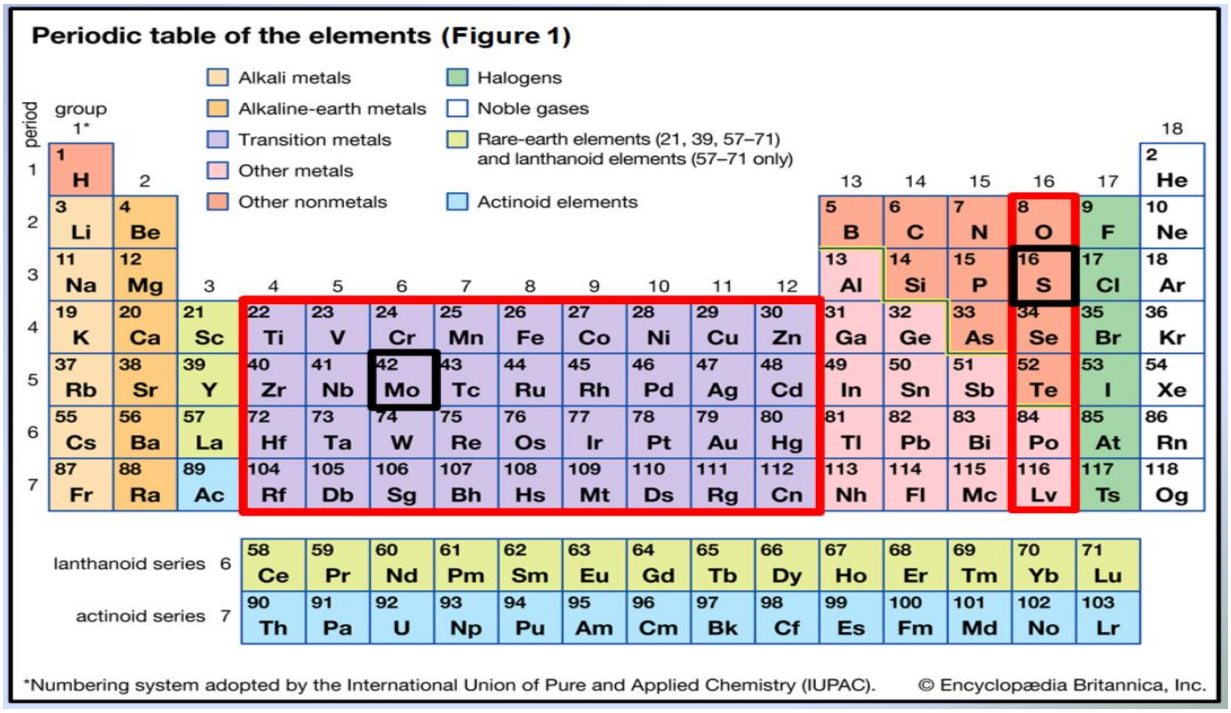

Figure 1.2. The periodic table which represents transition metals and chalcogens.
SOURCE: Encyclopaedia Britannica, Inc.

TMDCs have electronic properties ranging from semiconducting to superconducting depending upon chemical composition. Group-VI TMDCs monolayers (e.g., MoS_2, WS_2, $MoSe_2$, and WSe_2) exhibit semiconductor behavior .Recently TMDCs have drawn attention in many fields after the discovery of graphene and wide applications 2D nanomaterials in many fields. Recently TMDCs have drawn attention in many fields after the discovery of graphene and wide applications 2D nanomaterials in many fields.

1.3 Molybdenum disulfide (MoS_2)

MoS_2 is an inorganic compound composed of molybdenum and sulfur. It is a silvery black solid exists in natural in mineral molybdenite and have a hexagonal layered structure similar to graphite. It is a semiconductor with indirect band gap 1.2 eV (bulk) and a direct band gap of 1.8 eV (monolayer).

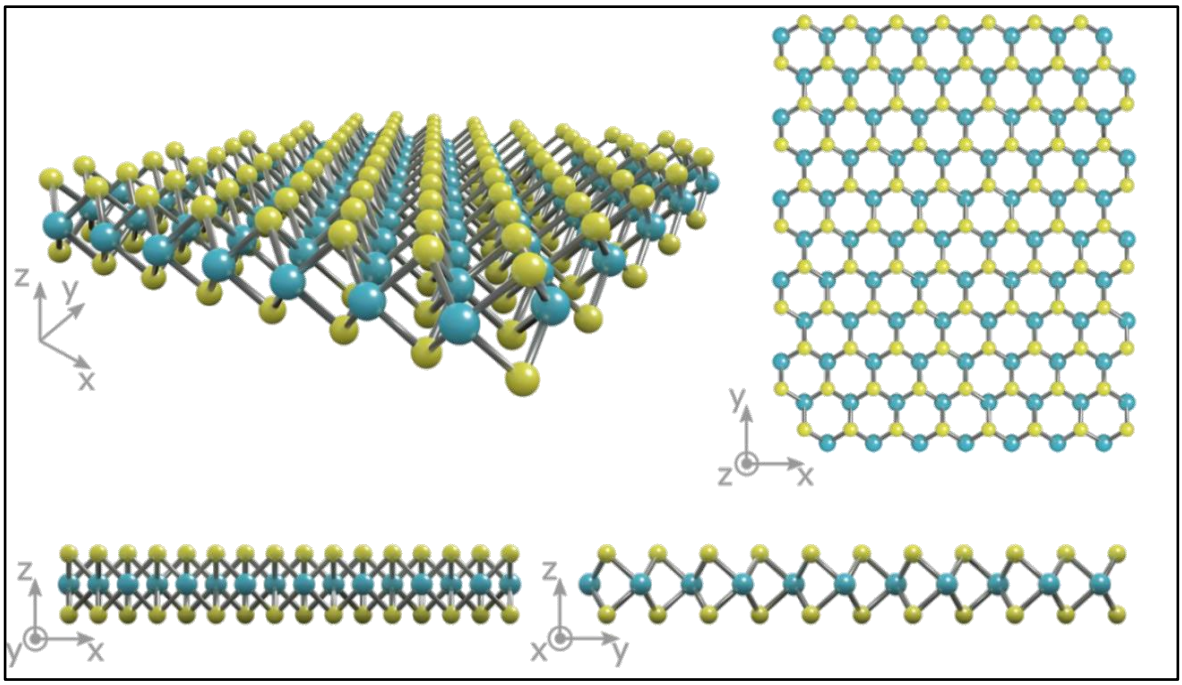

Figure 1.3 Crystal structure of monolayer MoS_2 showing a monolayer of molybdenum (blue) atoms sandwiched between two layers of sulfur (yellow) atoms. SOURCE: Molybdenum Disulfide, MoS_2: Theory, Structure & Applications | Ossila.

Generally, a single layer of MoS_2 has a laminar S-Mo-S structure with a thickness of approximately 0.7nm[2]. A single layer MoS_2 has a sandwich like structure with Mo atom in between two S atoms i.e. S-Mo-S. The unit cell of MoS_2 shows that the Mo atoms have a coordination of six, the sulfur has a coordination of three and exist in a trigonal prismatic D_3h space group[3]. Coordination of the Mo metal and its d-electrons play an important role in manipulating the electronic property of MoS_2 nanosheets[4].

A single layer has a trigonal prismatic (2H) or octahedral (1T) metal coordination phase. In phases 1T, 2H, and 3R the number indicates the number of layers in the crystallographic unit cell and the letter indicates the type of symmetry. T stands for tetragonal, H stands for hexagonal and R for rhombohedral[5] .

1T-MoS_2 is a metastable crystalline phase having tetragonal symmetry and is metallic. 1TMoS_2 monolayer is a slab of hexagonal Mo lattice occupies at the centre by octahedral coordination between two layers of hexagonally packed S atoms[6]. In both 2H-MoS_2 and 3RMoS_2 phases each Mo atom is covalently bonded to six surrounding S atoms forming a trigonal prismatic coordination[7].

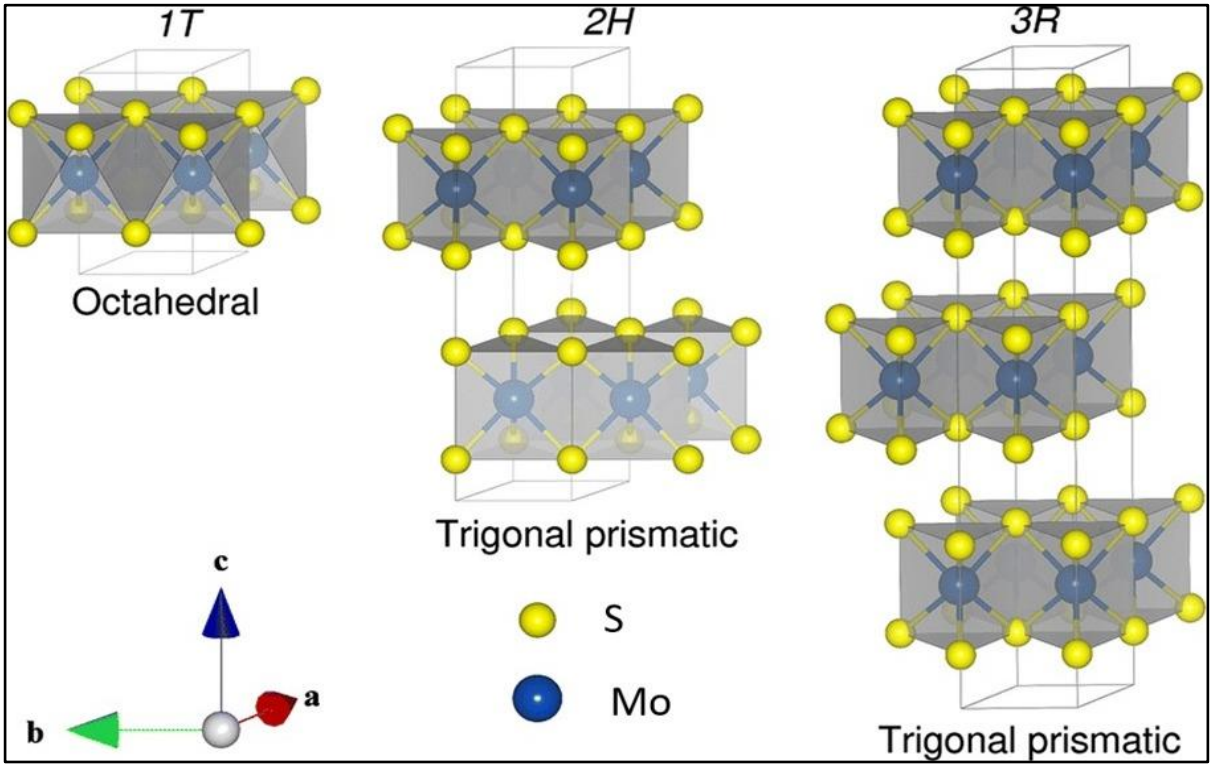

Figure 1.4. Crystal structure of MoS_2: Octahedral(1T), Trigonal Prismatic (2H) and Trigonal Prismatic (3R) unit cell structures. SOURCE: MoS_2 as a co-catalyst for photocatalytic hydrogen production from water by Bing Han.

2H-MoS_2 consists of two hexagonal planes of S atoms and an intermediate hexagonal plane of Mo atoms coordinated through ionic-covalent interactions with the S atoms in a trigonal prismatic arrangement[8].

In 3R-MoS_2 arrangement of S-Mo-S layers are similar with a significantly shifted relatively each other in comparison with 2H-MoS_2[9].

The bandgap of single layer 2H-MoS_2 is found to be double than that of bulk 3R-MoS_2. 2H-MoS_2 phase is more stable at high temperature as compared to 3R-MoS_2[10].

The optical bandgap transforms from indirect to direct one when the dimensions of MoS_2 is reduced from bulk to monolayer sheet. The indirect bandgap become larger while decreasing number of layers dur to quantum confinement effect in c axis direction[11]. The unique bandgap properties lead into better application in devices such as solar cell, FET, and photoluminescence[12 13].

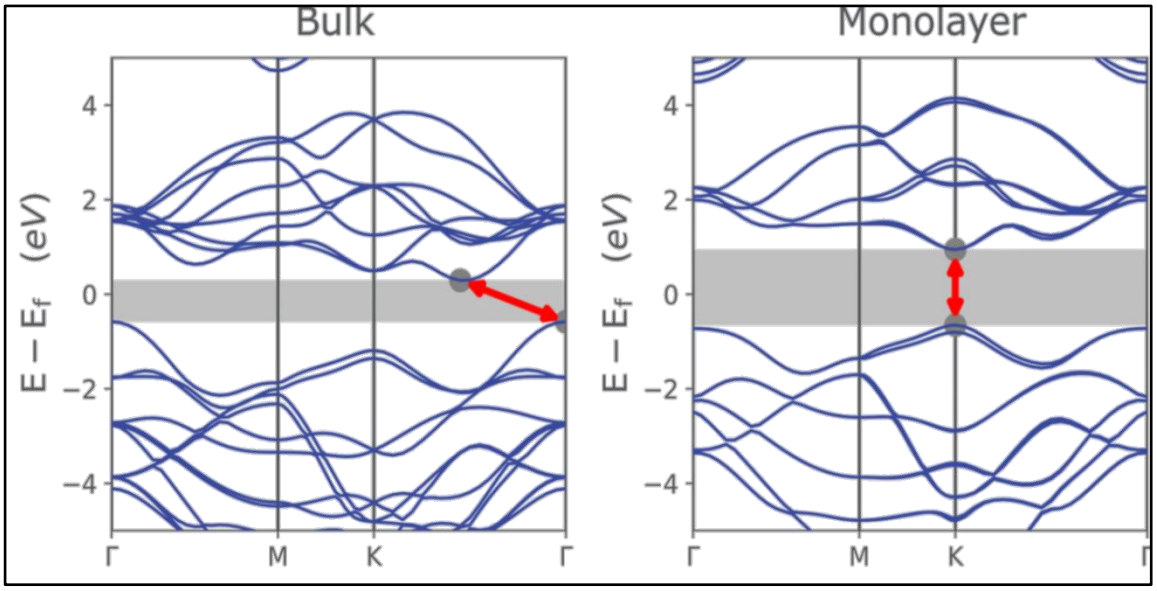

Figure 1.5. Band diagram of bulk and monolayer MoS_2 showing crossover from indirect to direct bandgap accompanied by a widening of the bandgap. SOURCE: Molybdenum Disulfide, MoS_2: Theory, Structure & Applications | Ossila.

In bulk form, the weak interlayer interactions allows sheets to easily slide over one-another, so it is often used as lubricant[14]. Semiconductor nature of MoS_2 can be described by group theory and ligand field theory using prismatic MX6 prisms as a model[15]. MoS_2 monolayer transistors generally display n-type behaviour with carrier mobilities approximately 350 $cm^2 V^{-1} s^{-1}$ [16].

Table 1.1 Basic Properties of MoS_2

Chemical Formula	**MoS_2**
Band gap	1.23 eV (direct, bulk) 1.8 eV (indirect, monolayer)
Molar mass	160.7 g mol^{-1}
Density	5.06 g cm^{-3}
Melting point	1185ºC
Solubility	Insoluble in water

1.4 Applications

1.4.1 FETs (Field Effect Transistor)

A finite Schottky barrier and large contact resistance between monolayer MoS_2 and electrodes are main aspects for developing field-effect transistors. Very large bandgap makes molybdenum disulfide as a suitable option for FETs. MoS_2 based FET has been demonstrated to exhibit high ON/OFF ratio exceeding 10^8 .

1.4.2 Gas Sensor

MoS_2 is excellent material for sensor applications due to the extraordinary physical and chemical properties. It is viable because of its capabilities of lower detection limits and selective detection of certain gases and also given its superior semiconductor properties and larger surface-to-volume ratio.

1.4.3 Lubricants

Molybdenum disulfide is largely used as lubricants because of its layered structure and the materials can shear more easily parallel to these layers. Thus, can bear heavy loads while still sliding.

1.5 Preferred Synthesis Method (Thermal CVD)

Out of the various synthesis methods, which is later mentioned in the next chapter, the preferred synthesis method is dual-zone thermal chemical vapour deposition (CVD).

CVD is one of the most commonly used method to fabricate 2D materials with large area and uniform thickness. It is used for producing composite material films in producing of different nanomaterials. Advantageous attributes of CVD is formation of high quality, high purity, high performance solid materials with fine structural regularity[17] [18]. Deposition of material onto the substrate is multidirectional.

It is a promising method to engineering physical, chemical and mechanical properties of surfaces. To deposit a material as thermal coatings, the mechanical, thermal properties and phase stability such as thermal stability plays an important role[19]. The operating parameters, modes and conditions can be selected based on the base materials and application. It is a highly controllable method to synthesis monolayer nanomaterials onto substrate.

1.6 Objective of Thesis

Temperature-dependent Raman spectroscopy of monolayer MoS_2 has been studied here to understand the effect of different temperatures on different Raman modes. The monolayer of MoS_2 were characterized using optical microscopy, scanning electron microscopy (SEM), X-ray diffraction (XRD) and Raman spectroscopy. The MoS_2 sample were prepared using a chemical vapour deposition (CVD) method and its structural features were examined by Raman Spectroscopy at different temperatures (273K to 573K). Furthermore, our temperature-dependent Raman spectroscopy reveals that as the temperature rises from 273K to 573K, the softening of Raman modes (Grüneisen parameters) E^1_{2g} and A_{1g} occurs due to anharmonicity and a negative temperature coefficient which tells us that the thermal conductivity and electrical resisitivity decreases as temperature increases.

This behaviour can be described by a double resonance mechanism that occurs in monolayer and few layer thick nanosheets. The frequency shifts and peak broadening of a monolayer MoS_2 can give clear, nondestructive, and accurate information. Raman spectroscopy can also be used to characterizing the structural, optical, electrical, and vibrational characteristics of other 2D layered materials.

Chapter 2

Synthesis Techniques

This chapter discusses briefly about the various methods that can be used to synthesize MoS_2 monolayer. Topdown and bottom-up are two different approaches in fabrication of nanostructures. Top-down techniques are well developed techniques but bottom-up techniques are rather more advantageous than former because it has better chance of producing nanostructures with less defects, more homogeneous chemical composition and able to build smaller structures.

2.1 Top-Down Approaches

A top-down synthesis method in which nanostructures are synthesized by etching out crystals planes which are already present on the substrate. It provides consistency in terms of particles size, shape and geometry.

2.1.1 Micromechanical Exfoliation

It is the simplest of methods and makes use of weak vdW forces. A scotch tape is used to peel off the layers of MoS_2 from bulk material. The tape is then pressed onto a substrate. The peeled off layer is transferred onto the substrate by vdW forces between them (Novoselov & Castro Neto, 2012)[20]. The disadvantage of this method is its limitation to lab scale.

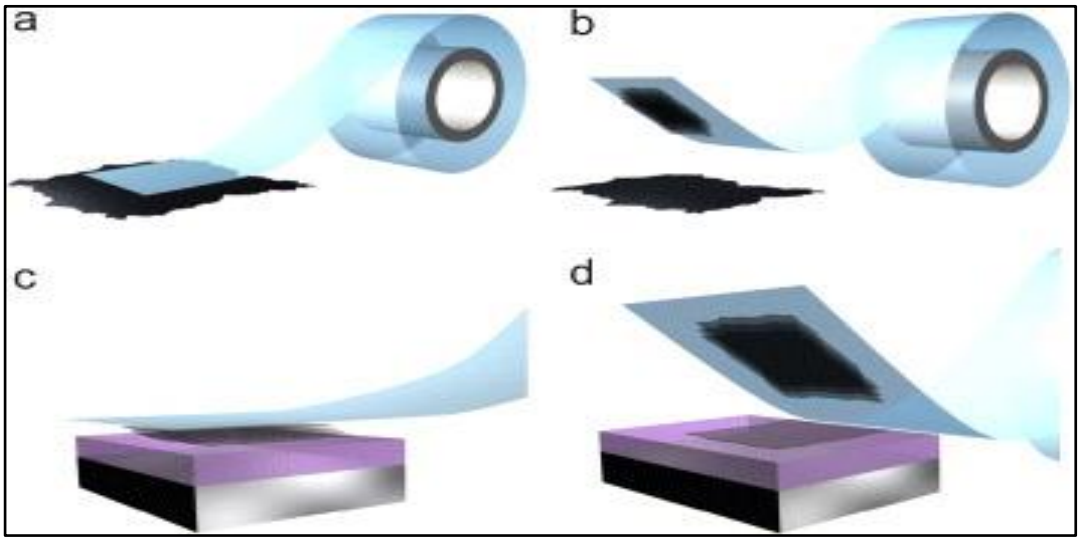

Figure 2.1. (a) Scotch tape pressed onto bulk crystal, (b) Scotch tape peeled off, bringing multiple atomic layers with it, (c) Multilayers pressed onto desired substrate and (d) Tape peeled off again, leaving a single atomic monolayer behind. SOURCE: (Novoselov & Castro Neto, 2012).

2.1.2 Liquid Phase Exfoliation

This process begins from bulk MoS_2, producing flakes with random shapes, sizes and number of layers. Broadly there are 2 routes to exfoliate MoS_2 in solution:

1) Mechanical i.e., by sonication, shearing, stirring, grinding and bubbling. It is a purely physical process and surfactants need to be added only to prevent exfoliated flakes from recombining.)
2) Atomic intercalation-Lithium is typically used to intercalate between the MoS_2 layers and enlarge the interlayer spacing, easing the following exfoliation by mechanical treatment (e.g., sonication).

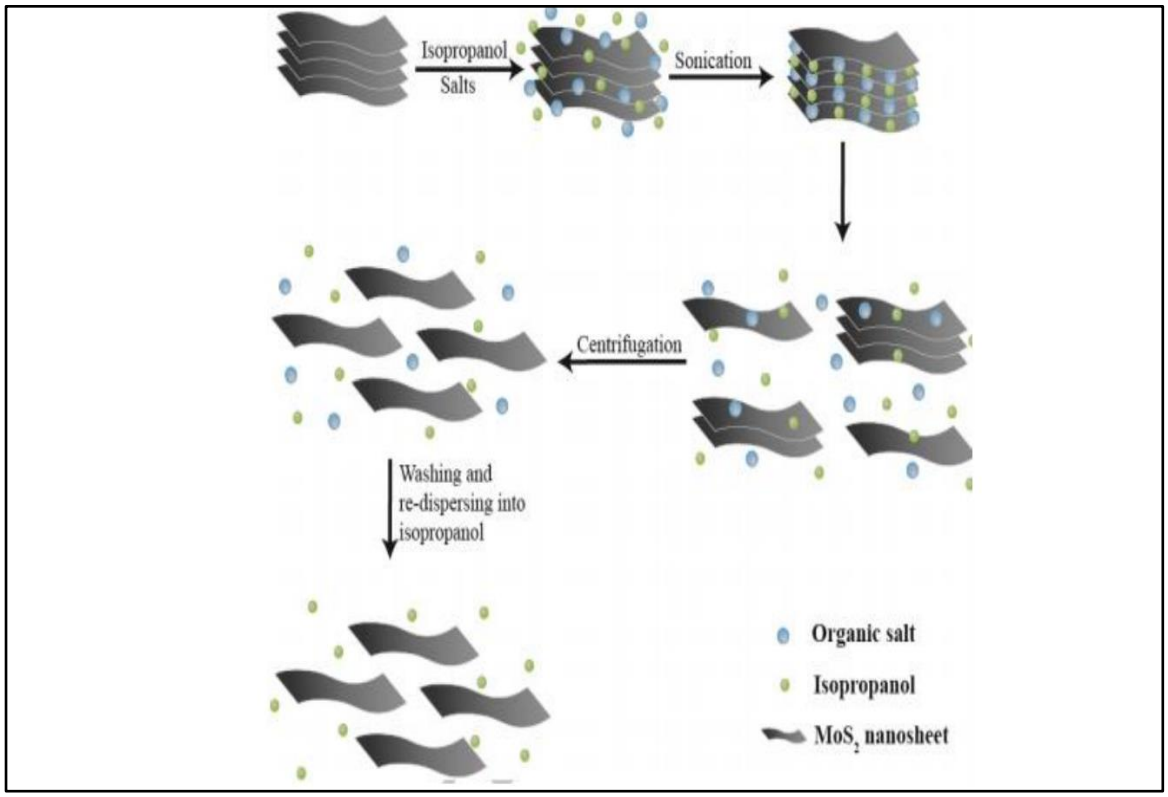

Figure 2.2. Step by step graphical representation of Liquid phase exfoliation method. SOURCE: (Huaizhi Liu et al., 2018).

The disadvantages of exfoliation process is that the quality of flakes obtained is poor even though yield is higher as compared to mechanical exfoliation. This method also results in loss of semiconducting properties due to the structural changes during Li intercalation. This can be resolved by annealing above 300° C. It is a cost effective method to produce low quality, large quantity nano flakes at industrial level.

2.2 Bottom-Up Approach

A bottom-up approach implies the nanostructures are synthesized onto the substrate by stacking atoms onto each other which give rise to crystal planes, crystal planes further stack onto each other, resulting in formation of nanostructures. This approach is advantageous than the former in many aspects be it size constraints, etc.

2.2.1 Chemical Vapor Deposition

By far the most compatible method for MoS_2 thin film synthesis whereby the precursors are allowed to vaporize at high temperatures in an inert gas environment, which then deposit on the substrate of choice.

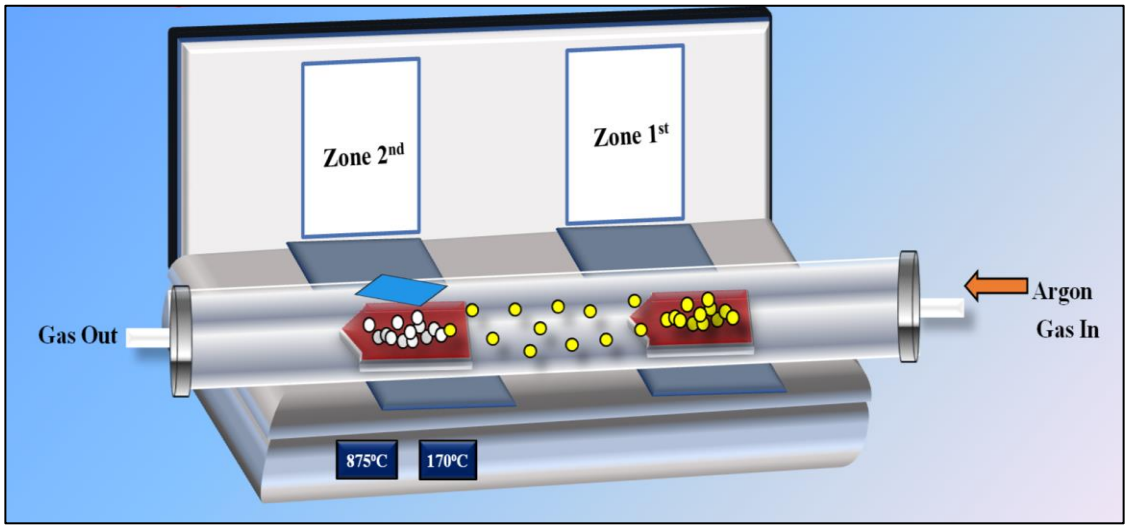

Figure 2.3. A schematic Chemical Vapour Deposition process.

The vaporized sulfur and molybdenum trioxide react as follows (Sun et al., 2017)[21].

$$MoO_3 + 2H_2S + H_2 = MoS_2 + 3H_2O \quad \text{..... (2.1)}$$

$$8MoO_3 + 24H_2S = 8MoS_2 + 24H_2O + S_8 \quad \text{..... (2.2)}$$

$$16MoO_3 + 7S_8 = 16MoS_2 + 24SO_2 \quad \text{..... (2.3)}$$

2.2.2 Solution Chemical Process

Hydrothermal synthesis and solvothermal synthesis typically use molybdate to react with sulfide or just sulfur in a stainless steel autoclave, where a series of physicochemical reactions take place under relatively high temperature (e.g., 200° C) and high pressure for several hours or longer.

The resultant is MoS_2 powders of different shapes. The size of individual particles can be adjusted to some extent. Very frequently, the powders are post-annealed to high temperature, to improve their crystalline quality and purity. The only difference between hydrothermal and solvothermal synthesis is that the precursor solution in the latter case is usually not aqueous. Other solution chemical processes start at around room temperature and atmospheric pressure, where postannealing is often used anyway. The products can be either a powder or thin film, depending on the preparation details. The most commonly-used precursor is $(NH_4)2MoS_4$ (ammonium tetrathiomolybdate), or sodium molybdate. $(NH_4)2MoS_4$ decomposes to form MoO_3 at 120-360 °C, which can be further converted into MoS_2.

2.2.3 Physical Vapor Deposition (PVD)

It is a vaporization coating technique in which the material goes from a condensed phase to a vapor phase and then back to a thin film condensed phase. The most common form of physical vapor deposition are thermal evaporation, magnetron sputtering, and arc vapor deposition. The process involves four steps: (i) evaporation of the material to be deposited; (ii) transport of the vapor to the substrate to be coated; (iii) reaction between metal and respective reactive gas during transport; (iv) deposition of coating at substrate surface.

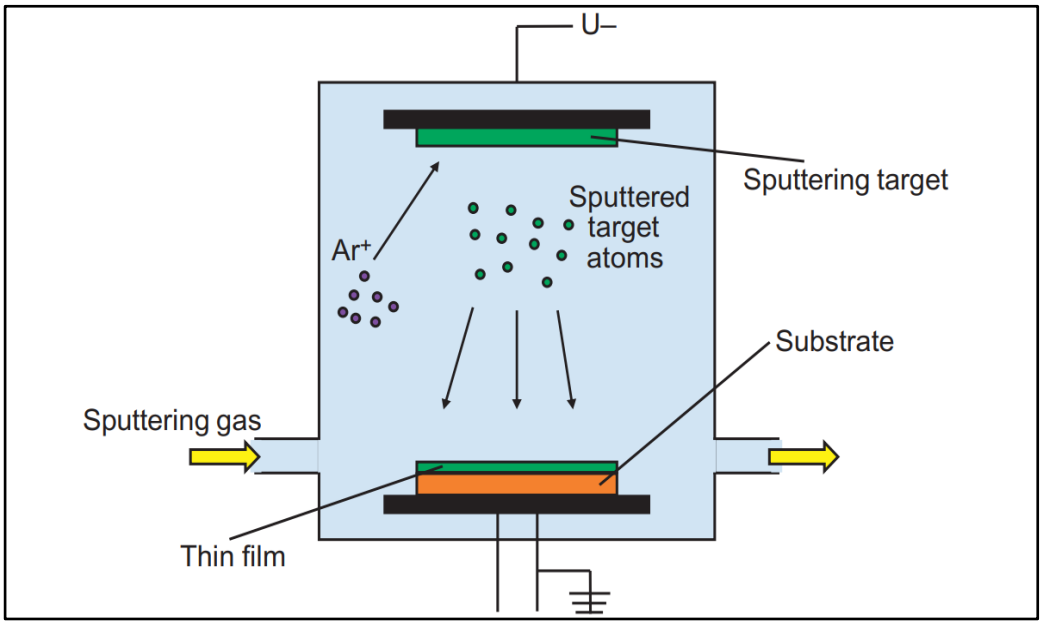

Figure 2.4. Schematic illustration of a typical physical vapor deposition process. SOURCE: https://doi.org/10.1016/B978-0-12- 813518-1.00020-5.

Chapter 3

Characterization Techniques

This chapter will discusses the various characterization approaches that can be applied to examine the final product created during the synthesis process and assess whether the expected outcomes were achieved or not.

We will discuss different techniques, instrumentations used, their working principles and the information they provide. Also, we will discuss how to interpret the raw data/information obtained during analysis to reach to certain conclusions.

The details of characterization used for this work are as follows:

3.1 Optical Microscopy

Optical microscopy is a technique that allows the viewing of samples more closely using optical microscopes. It relies on light and one or more lenses to magnify samples. Optical microscopy is remarkably versatile, increasing the detail and contrast of a microscopic specimen.

3.2 Scanning Electron Microscopy(SEM)

A type of electron microscope known as a scanning electron microscope creates images of a specimen by employing raster scanning and a focused electron beam to move over the specimen's surface.

- An SEM creates magnified images of the specimen by probing along a rectangular area of the specimen with a focused electron beam. This process is called the raster scanning.
- It is called a scanning electron microscope because the image is formed by scanning the surface of the specimen in a raster pattern using a focused electron beam.
- SEM relies on the secondary emission of electrons from the surface of the specimen to achieve magnified image to be viewed.
- The major advantage of a SEM over TEM is that it can produce detailed image of the whole organisms and surfaces of the cells.

Figure 3.1. Scanning Electron Microscope setup.
SOURCE: MICROSCOPEWIKI.

A scanning electron microscope works on the principle of targeting a focused beam of electrons moving with high kinetic energy on a specimen.

3.2.1 Working principle of SEM

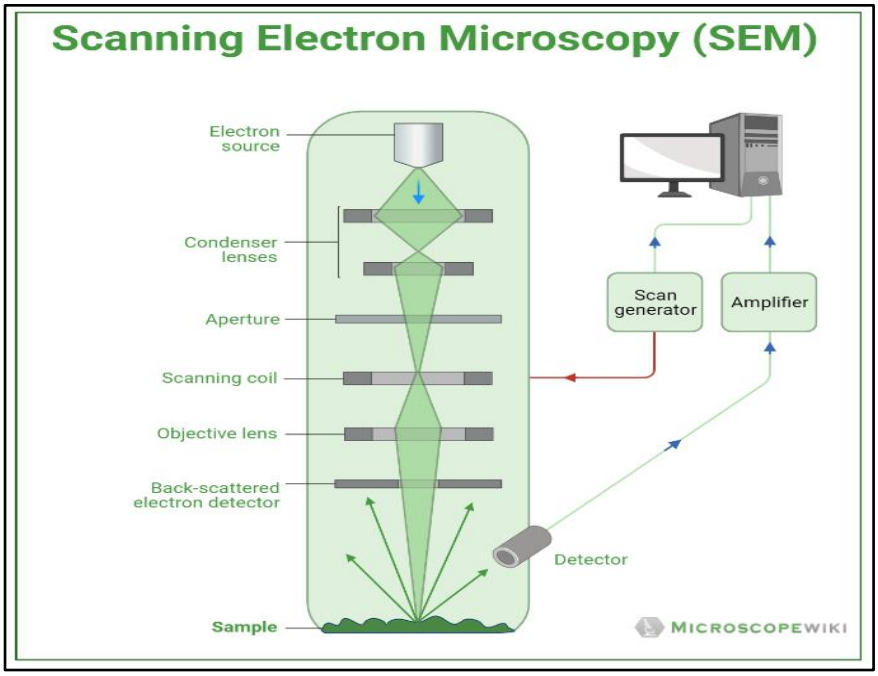

Figure 3.2. Working Principle of SEM. SOURCE: MICROSCOPEWIKI.

A scanning electron microscope works on the principle of targeting a focused beam of electrons moving with high kinetic energy on a specimen.

When these electrons scan the surface of the specimen, electrons are scattered and these secondary electrons that are slowed down on the impact of hitting the surface of the specimen are collected by a detector and these secondary electrons create the magnified image of the specimen thereby illustrating the morphology and topology of the specimen.

Similarly, the backscattered electrons from the surface of the specimen help us in illustrating the difference in composition of the specimen thereby making this type of microscope a useful instrument.

3.3 X-Ray Powder Diffraction (XRD)

X-Ray powder diffraction (XRD) is an important method to determine the atomic and molecular structure of a crystal. XRD diffractogram of a sample can provide information like strain, dislocation density, inter planar spacing, miller indices, etc. It works on the principle of diffraction/ reflection and follows Bragg's Law $n\lambda = 2d \sin\theta$ (Humphreys, 2013)[22].

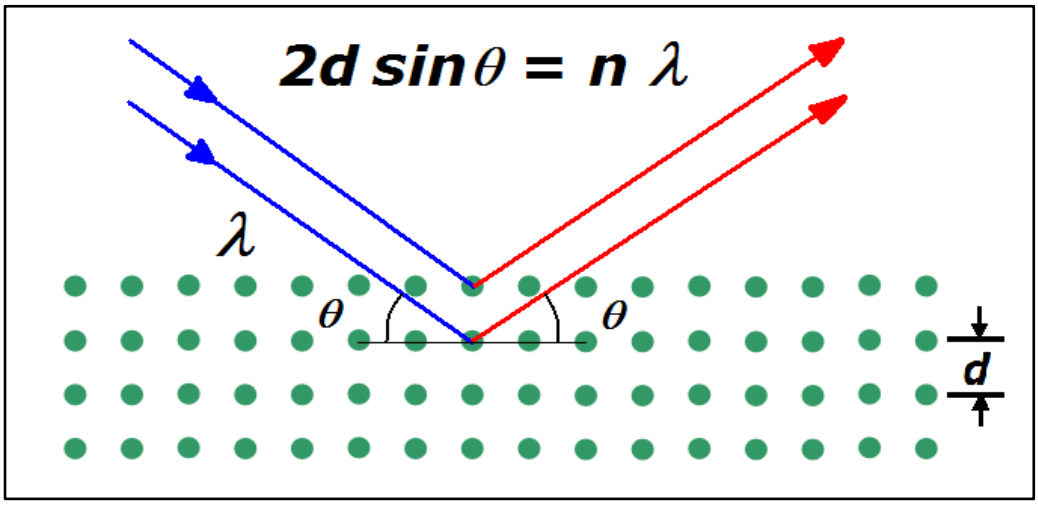

Figure 3.4 Diffraction of the incident X-ray beam by atomic planes in a crystalline solid can result in enhanced signals if all the waves undergo constructive interference. This can be accomplished if there is an integral wave value (n), as determined by Bragg's law. SOURCE: Venkat Sunil Kumar Channam.

Whenever an X-ray of wavelength λ is incident on a crystal, with inter planar spacing d, at an angle θ, it diffracts from the atoms in that plane. All these diffracted radiations interfere to give an nth order signal, which is collected by a detector.

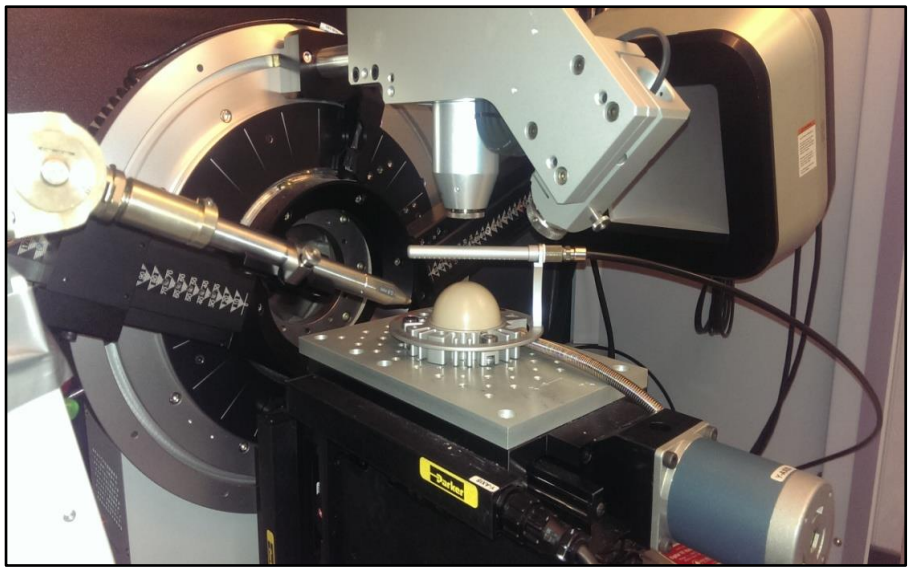

Figure 3.5 A powder X-Ray diffractometer. SOURCE: The University of Chicago.

3.4 Raman Spectroscopy

Raman spectroscopy is very appropriate, nondestructive and advanced technique used to characterize the structural, mechanical and vibrational properties of layered material. This is the ultimate test for confirmation of any material. This is because each molecule or material has a unique Raman spectrum. Raman spectroscopy is commonly used in chemistry to provide a structural fingerprint by which molecules can be identified.

Raman spectroscopy relies upon inelastic scattering of photons, known as Raman scattering. A source of monochromatic light, usually from a laser in the visible, near infrared, or near ultraviolet range is used, although X-rays can also be used. The laser light interacts with molecular vibrations, phonons or other excitations in the system, resulting in the energy of the laser photons being shifted up or down. The shift in energy gives information about the vibrational modes in the system.

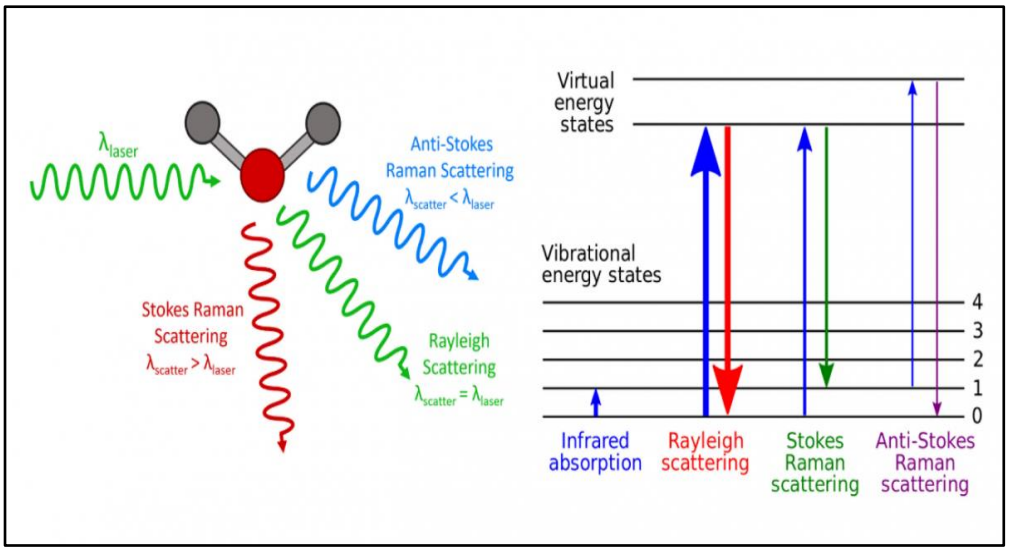

Figure 3.6 Visual representation of laser-induced molecular vibration and Raman scattering effect. SOURCE: Planetary Terrestrial Analogues Library.

When a high intensity laser source is made incident on a sample. The molecules within scatter this incident light. Most scatterings are Rayleigh scattering whereby the incident and scattered radiation have same wavelength.

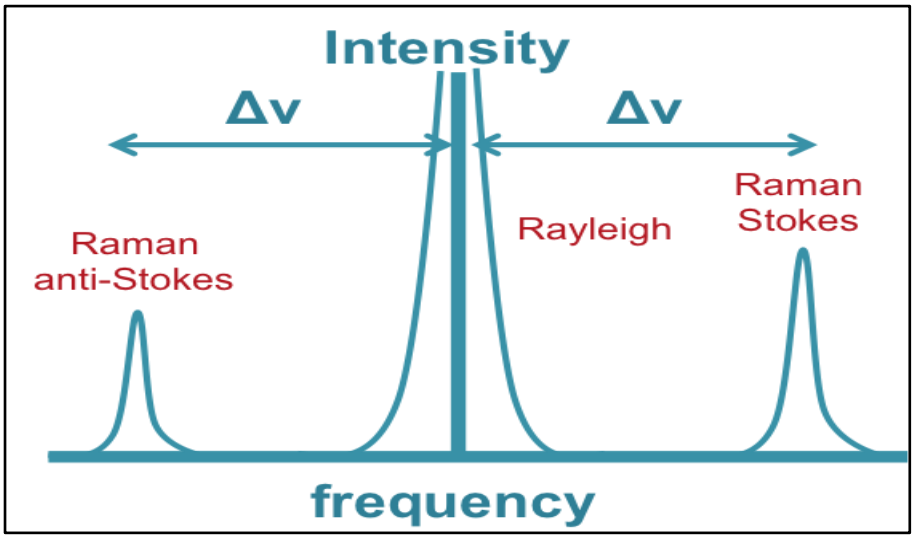

Figure 3.7 Three types of scattering processes that can occur when light interacts with a molecule. SOURCE : (Edinburgh Instruments, n.d.).

However a small percentage (0.0000001%) of light is scattered at wavelength different from the incident radiation. This is Raman Scattering (Raman & Krishnan, 1928) and highly depends on the material. Each peak in the Raman spectrum corresponds to a specific molecular bond vibrations.

3.5 X - Ray Photoelectron Spectroscopy (XPS)

X-ray photoelectron spectroscopy (XPS), also known as ESCA (electron spectroscopy for chemical analysis) is a surface analysis technique which provides both elemental and chemical state information virtually without restriction on the type of material which can be analysed. It is a relatively simple technique where the sample is illuminated with X-rays which have enough energy to eject an electron from the atom. These ejected electrons are known as photoelectrons[23].

The kinetic energy of these emitted electrons is characteristic of the element from which the photoelectron originated[24]. The position and intensity of the peaks in an energy spectrum provide the desired chemical state and quantitative information. The surface sensitivity of XPS is determined by the distance that that photoelectron can travel through the material without losing any kinteic energy.

These elastiaclly scattered photoelectrons contribute to the photoelectron peak, whilst photoelectrons that have been inelastically scattered, losing some kinetic energy before leaving the material, will contribute to the spectral background[25].

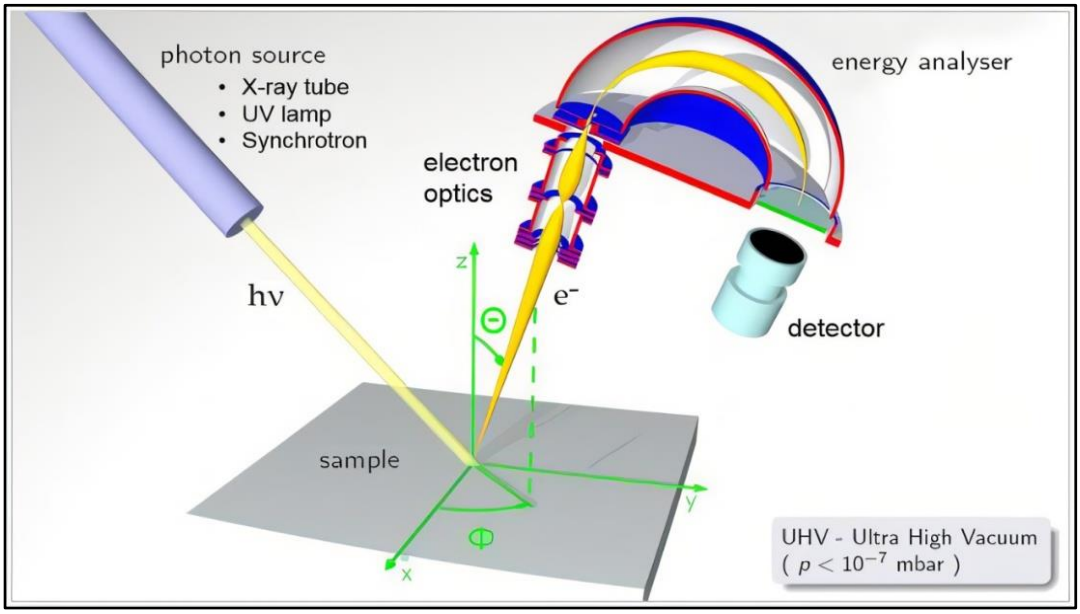

Figure 3.8 Schematic of X-Ray Photoelectron spectroscopy. SOURCE: Yale University, n.d.

Chapter 4

Experimental Techniques

The chapter discusses the details of growth of MoS_2 on SiO_2 using CVD method.

Firstly, literature review of previous research works regarding the CVD synthesis of monolayer MoS_2 is carried out in order to have a better idea and aspects for proceeding with the experiment.

4.1 Setup of Equipments

Figure 4.1. Thermal CVD equipment used for synthesis in laboratory.

Before proceeding within the experiment, the setup of all the equipment has to be done. The quartz tube be placed between the coils and fixed. Nitrogen/Argon cylinders to be fitted with regulator knob and tubes for connection in quartz tube. The quartz tube has to be handled very carefully. Proper and safe electrical connection are provided to the CVD with MCBs for extra safety. Water to be filled at the required level in the ultrasonication baths[26].

The CVD which we are using for performing the synthesis is a dual zone CVD with a low temperature zone and other high temperature zone which makes it favorable for vaporizing and chemically reacting precursors with different melting point at the same time.

Rotameters are connected at the ends of the quartz tube to measure and regulate pressure inside of the quartz tube.

4.2 Materials & Apparatus Used

Table 4.1 Materials and Apparatuses used

Precursor	➢ Molybdenum trioxide (MoO_3) powder ➢ Sulphur (S) powder
Substrate	➢ Silicon dioxide (SiO_2) wafer
Apparatus	➢ Ceramic Combustion Boats ➢ Butter paper (for weighing precursors) ➢ Weighing Machine (with milligram scale) ➢ Ultrasonication Bath ➢ Rotameter (to measure and control flow of gas)
Cleaning Reagents	➢ Deionized (DI) water ➢ Acetone ➢ Isopropyl Alcohol (IPA) ➢ Methanol ➢ Piranha Solution (3 parts conc. H_2SO_4 and 1 part 30% H_2O_2)
Carrier Gases	➢ Nitrogen ➢ Argon

4.3 Prerequisite

After setting up equipment, all the apparatus and substrates are to be cleaned thoroughly to prevent any impurities form getting the desired results and affect the end product.

4.3.1 Cleaning substrate (SiO_2)

i. SiO_2 substrate is put into Piranha solution and then in DI water for cleaning any inorganic impurities off the substrate.

ii. Substrate is put in a beaker filled with methanol and placed in ultrasonication bath for 5 mins at 50ºC.

iii. Then put in a beaker filled with acetone, undergoes ultrasonication for 5 mins at 50ºC.

iv. At last, put in deionized (DI) water and ultrasonicated for 5 mins. These last three steps are further repeated 2-3 times to makes sure that no impurity is left on the substrate.

4.3.2 Cleaning Ceramic boat

i. Ceramic boats are washed thoroughly with soaps and any other previous depositions are removed by scratching it.

ii. Boats are filled with acetone and then ultrasonicated at 50ºC for 5 mins.

iii. Then boats are filled with methanol and again placed in ultrasonication for 5mins at 50ºC.

iv. Lastly, boats filled with DI water are placed in ultrasonication bath for 5 mins at 50ºC. (Last two steps are repeated 2-3 times simultaneously.)

4.3.3 Cleaning Quartz tube

By products from the previous operations resides on the inner side of the tube which needs to be cleaned to avoid any alter in the end products. IPA (Iso Propyl Alcohol) is used to clean the quartz tube inside with the help of a dusting cloth and a log rod that is long enough to clean it thoroughly.

4.3.4 Weighing Precursors and Placing in Ceramic Boats

Precursors are measured carefully using a weighing scale with milligram scale. First a clean weighing paper/ filter paper is placed on the weight machine and then it is tared to see a

reading of zero. Now precursor is placed in very small quantities as required with the help of a clean spatula.

The precursors (MoO_3 and S) are put into two separate cleansed ceramic combustion boats and spread thoroughly in the boat bed with the help of spatula.

4.4 Synthesis Process

After setting up all the instruments and performing the prerequisites, experiment is started. The CVD used is programmable so the temperature and time periods are preprogrammed with the help of controller and verified for any discrepancies.

4.4.1 Steps involved in CVD operation

i. The ceramic boat with MoO_3 (Molybdenum Trioxide) powder and faced-down SiO_2 (Silicon dioxide) was placed above high temperature zone (Zone 2) inside the quartz tube with help of a long rod curved at the end[27].

ii. Place the other ceramic boat with S (Sulphur) powder above the low temperature zone (Zone 1).

iii. Insert the cotton-based insulator at both the ends of the tube and seal both ends with caps and screws.

iv. Rotameters are connected at both the ends for monitoring and controlling the inflow of the inert gas through the quartz tube. Rotameter at the side of Zone 1 is connected to the cylinder knob.

v. CVD is started and the gas flow is monitored throughout the process.

vi. After the process is completed, the CVD is turned off and gas flow stopped to let it cool off for 5-6 hours.

vii. Boats are taken out after cooling of the CVD and the substrate is taken for observation.

4.4.2 Growth Process

Prior to starting the experiment for 15 mins gas was flown through the tube to maintain a neutral environment inside the tube. The temperature rises with time in both the zones and

reaches the melting point of both the precursors (i.e., 120ºC for sulfur and 875ºC for molybdenum trioxide) which starts to vaporize.

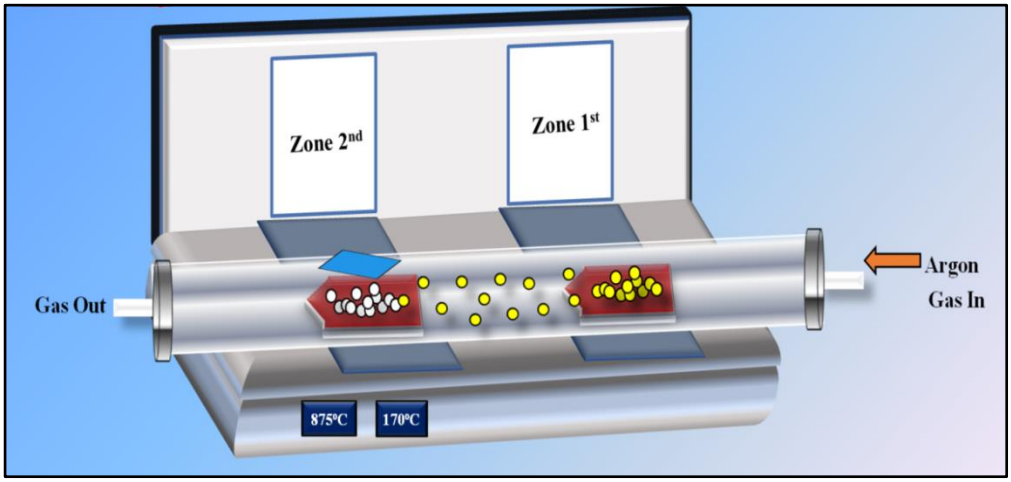

Figure 4.2 Schematic representation of the CVD process.

Vapors of the precursors are carried together and chemically react with each other and deposits over the surface of the substrate to form molybdenum disulfide (MoS_2). In deposition period the temperature is kept constant and gas flow is maintained ~200 sccm which facilitates the deposition of product on the substrate film. Which further cools and forms a nanofilm over the substrate surface[28].

$$MoO_3 + 1/2S \rightarrow MoO_3 + 1/2SO_2 \quad \ldots\ldots (4.1)$$

$$MoO_3 + 3S \rightarrow MoS_2 + SO_2 \quad \ldots\ldots\ldots\ldots\ldots (4.2)$$

During the project work various samples were prepared by varying different parameters in order to observe the variation in end-product and get a better optimized output suitable[29].

The main parameters that affect the end product are the temperature inside both zones, time period, rate of gas flow, distance between precursors, and quantity of the precursors.

Table 4.2 Amount of precursors used for the synthesis of MoS_2.

Molybdenum trioxide (MoO_3)	**6 mg**
Sulphur(S)	**250 mg**

Table 4.3 CVD temperature and time period (Zone 1).

T1(ºC)	**T2(ºC)**	**Time1(mins)**
30ºC	65ºC	30
T2(ºC)	**T3(ºC)**	**Time(mins)**
65ºC	120ºC	60
T3 (ºC)	**T4(ºC)**	**Time(mins)**
120ºC	200ºC	10

Table 4.4 CVD temperature and time period (Zone 2).

T1 (ºC)	**T2(ºC)**	**Time2(mins)**
30ºC	550ºC	30
T2 (ºC)	**T3 (ºC)**	**Time(mins)**
550ºC	875ºC	60
T3 (ºC)	**T4 (ºC)**	**Time(mins)**
875ºC	875ºC	10

Table 4.5 Rate of Nitrogen gas flow throughout the process.

Time period	**Rate (sccm)**
Starting 40 mins	~500 sccm
Next 60 mins	~300 sccm
Last 10 mins	~>200 sccm

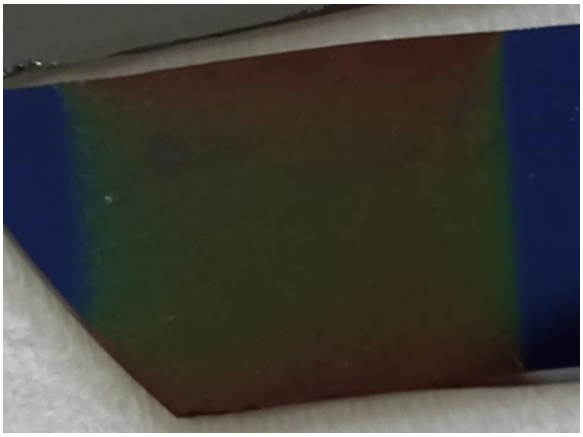

Figure 4.3 Substrate with deposition with deposition of MoS_2 on SiO_2

On increasing temperature, the evaporation pressure of MoO_3 increases thus more vapors of MoO_3 participate in CVD and hence more clear and better fabrication of MoS_2 are obtained. The rate of flow of carrier gas is maintained nearly same in all the attempts. Ratio of precursors i.e. MoO_3 : S is 1:50. After vary parameters and optimizing temperature, deposition of material is observed.

4.5 Precautions

While handling the equipment in the laboratory proper security measures should be taken. One must wear rubber gloves while cleaning the equipment and substrates as cleaning reagents in direct contact may harm skin and Piranha solution may cause deep skin burns. Much attention be given while using strong acidic or basic compounds[30].

Gas flow should be monitored properly at the outlet pipe also as sometimes deposition may lead to block the pipe or hole which can cause the quartz tube to burst and harm anyone nearby.

Chapter 5

Results & Discussion

In this chapter we would discussed the results obtained from the characterization of the samples produced by the various attempts as mentioned in previous chapter 4. The role of temperature on Raman Spectroscopy of MoS_2 monolayer under the effect of different temperatures on different Raman modes is discussed here in details.

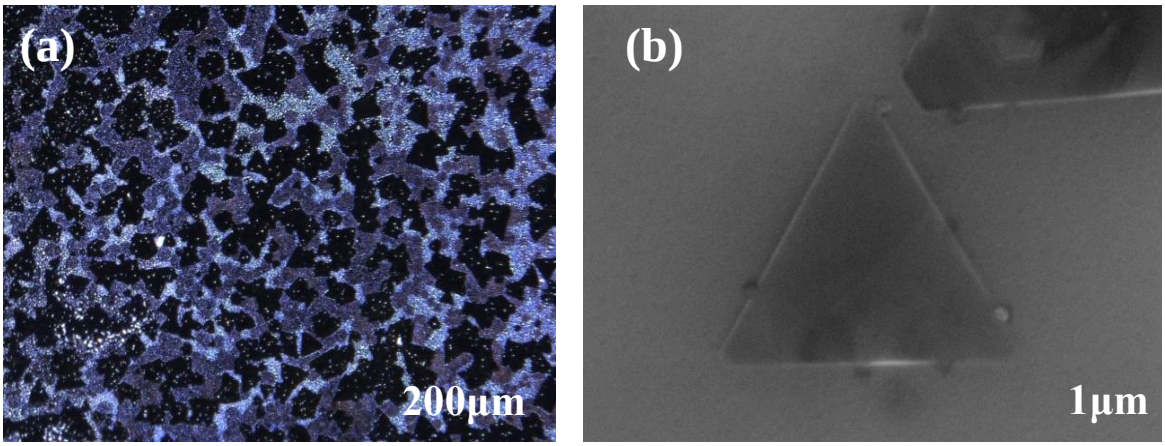

FIG. 5.1. (a) and (b) represents the Optical Microscopy and SEM images of monolayer MoS_2.

Figures. 5.1. (a) and (b) represents the optical microscopic and scanning electron microscope (SEM) images of monolayer MoS_2 prepared on 300 nm SiO_2 substrate respectively. The triangular domains in the SEM image confirms that the MoS_2 is monolayer.

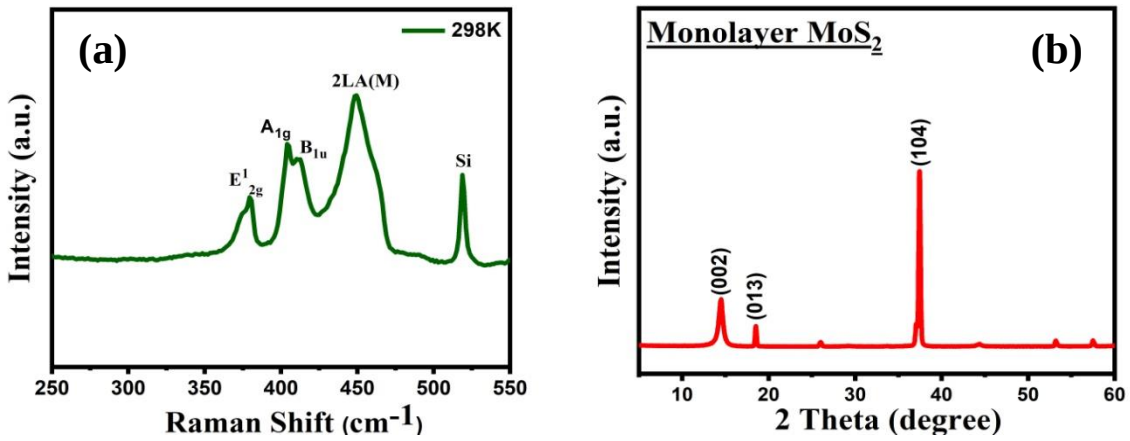

Figure 5.2. (a) Raman spectra of a monolayer MoS_2 observed at room temperature.(b) represents the X- Ray diffraction pattern of monolayer MoS_2 at room temperature.

Figure 5.2. (a) represents the Raman spectra of a MoS_2 monolayer observed at room temperature with a 633nm Ar laser are typical. The Raman spectra of MoS_2 show five distinct modes: E^1_2g, which arises at 379 cm^{-1}due to in-plane vibration, A_1g, which appears at 404 cm^{-1} due to out-of-plane vibration, 2LA(M) which appears at 449 cm^{-1}, B_1u which appears at 412 cm^{-1} and Si which appears at 518 cm^{-1} (b) represents the X- Ray diffraction pattern of few layer MoS_2 nanosheet on the SiO_2 substrate with the corresponding (hkl) plane at room temperature.

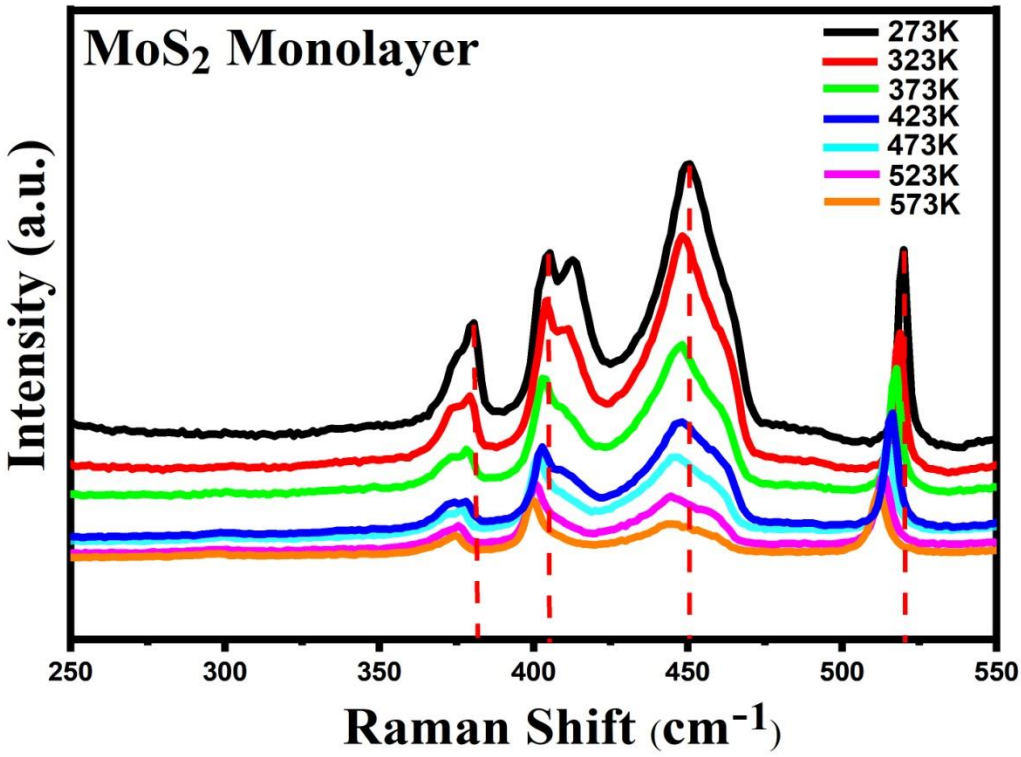

Figure 5.3. Raman spectra of monolayer MoS_2 sample observed at different temperatures ranging from 273K to 573K using 633nm laser.

Figure 5.3. shows the Raman spectra of a monolayer MoS_2 sample recorded at different temperatures ranging from 273K to 573K using 633 nm laser. When the temperature rises from 273K to 573K, the peak positions of E^1_2g, A_1g and 2LA(M) modes move to a lower wavenumber.

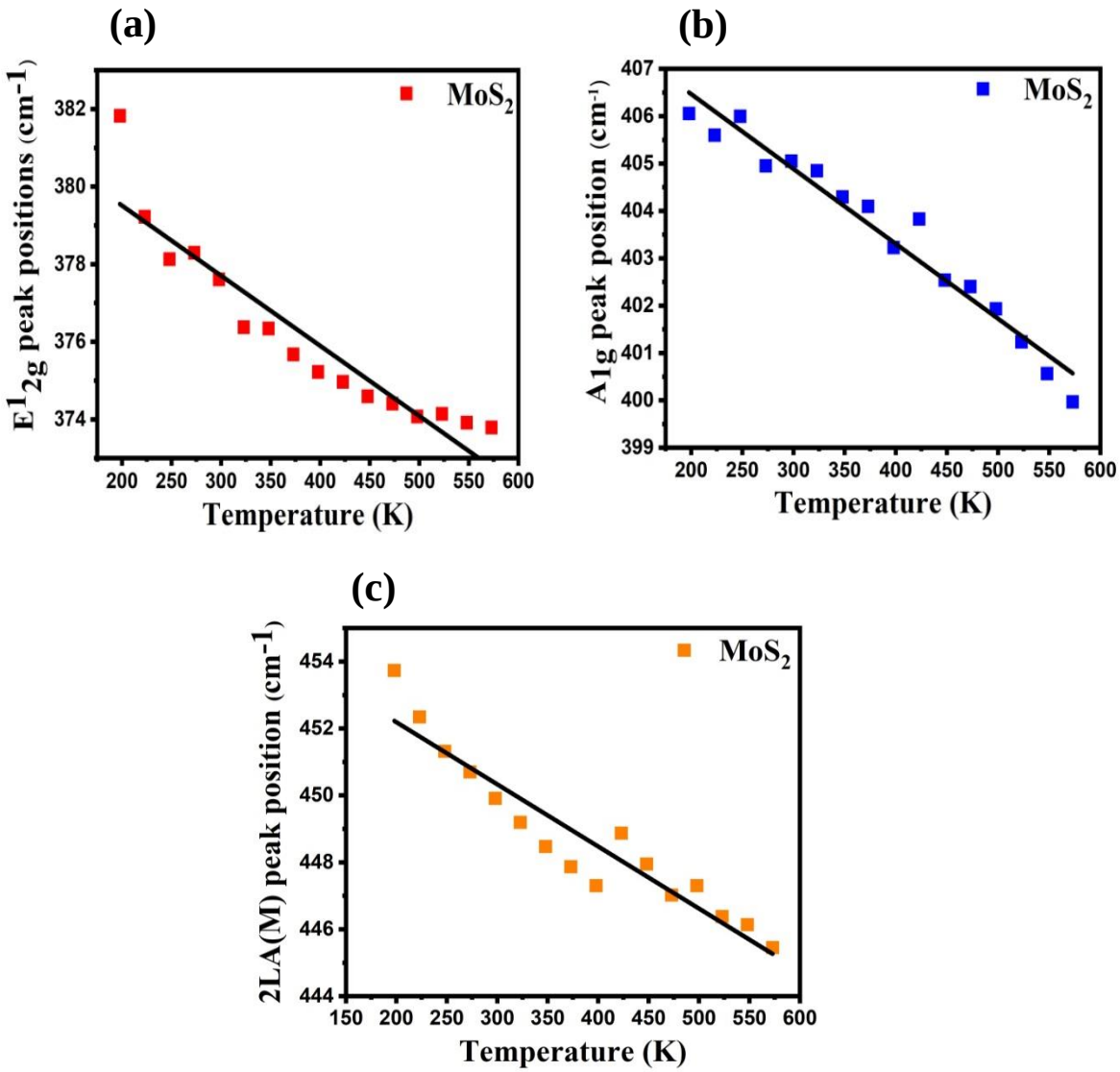

Figure 5.4. shows the Raman frequencies of a monolayer MoS_2 nanosheets as a function of temperature for (a) $E^1{}_2g$ mode, (b) A_1g mode and (c) 2LA(M) mode.

Figures 5.4. (a), (b) and (c) illustrate the Raman peak position shift as a function of temperature in $E^1{}_{2g}$, A_{1g} and 2LA(M) modes for MoS_2 monolayer sample at different temperatures.

It was found that some data points for Raman peak positions were spreading, which could be attributed to a change in laser spot on a monolayer MoS_2. The Raman modes $E^1{}_2g$ and A_1g of MoS_2 changes linearly with temperature as shown in the Figures. With increasing temperature, all monolayer MoS_2 modes 'FWHM' increases. Interactions between phonons and electrons are responsible for the observed behaviour. The anharmonicity as well as the thermal contribution both contribute to the shift in Raman-peak positions with temperature in

monolayer MoS_2. Temperature-dependent Raman spectra were also carried out on more monolayer MoS_2 sample, and the results were all consistent.

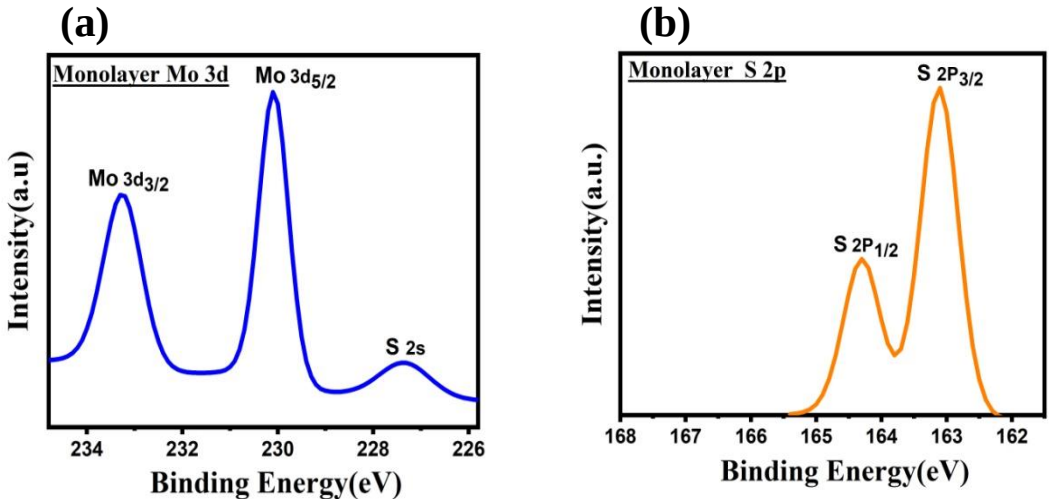

Figure 5.5. represents the XPS spectrum of (a) Mo_{3d} and S_{2s} (b) S_{2p} peaks of chemically derived monolayer MoS_2.

Figure 5.5. (a) The XPS spectrum for Mo3d and the S2s are displayed, along with their corresponding peaks. The Mo3d doublet with binding energies of 233.3 eV and 230.1 eV for the $Mo3d_{3/2}$ and $Mo3d_{5/2}$, respectively and the binding energy for S2s is 227.4 eV . These binding energies confirms that our sample is monolayer. (b) The S2p doublet X-ray photoelectron spectra are displayed, along with their corresponding peaks. The S2p doublet with binding energies of 164.3 eV and 163.1 eV for the $S2p_{1/2}$ and $S2p_{3/2}$, respectively.

The following equation was used to fit the data of the $E^1{}_2g$, A_1g and 2LA(M) mode peak positions versus temperature.

$$\omega = \omega_0 + \chi T, \quad \ldots\ldots\ldots\ldots \quad (5)$$

where ω_0 is the peak position of vibration $E^1{}_2g$, A_1g and 2LA(M) modes at zero Kelvin temperature and χ is the first- order temperature coefficient of $E^1{}_{2g}$, A_{1g} and 2LA(M) modes. The slope of the fitted straight line shows the value of the temperature coefficient χ, and the plot of $E^1{}_{2g}$, A_{1g} and 2LA(M) versus temperature yields a straight line. Temperature coefficients for the $E^1{}_2g$, A_{1g} and 2LA(M) modes of a monolayer MoS_2 were found to be -0.018 $cm^{-1}\ K^{-1}$, -0.015 $cm^{-1}\ K^{-1}$ and -0.018 $cm^{-1}\ K^{-1}$, respectively.

The temperature coefficients of a monolayer MoS_2 have been reported, and they correspond well with those of Sahoo et al., Najmaei et al., and Lanzillo et al..[31.] It's also worth noting that for a monolayer , the full width at half maxima (FWHM) of both $E^1{}_2g$ and A_1g peaks increases with rising temperature. A double resonance process, which is active only in one atomic thick layer and a few atomic layer thick nanosheets, could explain this result[32]. The observed pattern could be due to phonon-phonon interaction, in which a phonon decays into lower-energy phonons, and electron-phonon interaction, in which a phonon generates an electronhole (e-p) pair[33]. The following components contribution from thermal expansion or volume contribution and temperature contribution that results from anharmonicity were the main reasons for the deviation in the Raman spectra peak position of the normal modes as a function of increasing temperature[34] [35]. The interaction between the layers of MoS_2 nanosheets is known to be weak Van der Waals, which can be seen in the temperature coefficients of both Raman active modes. Thus, temperature-dependent Raman spectroscopy provides clear, nondestructive, and accurate information on frequency shifts, peak width variation, and changes in relative intensity of a monolayer MoS_2.

Chapter 6

Conclusion

6.1 Conclusion

In short, a for monolayer MoS_2 made using a chemical vapour deposition method, we examined the temperature dependent Raman spectroscopy behaviour. Our results shows that as the temperature rises from 273 K to 573 K, the E^1_{2g}, A_{1g} and 2LA(M) modes soften for a monolayer MoS_2. The first-order temperature coefficients of E^1_{2g}, A_1g and 2LA(M) modes for monolayer MoS_2 are **$-0.018\ cm^{-1}K^{-1}$, $-0.015\ cm^{-1}K^{-1}$** and **$-0.018\ cm^{-1}\ K^{-1}$**, respectively. The results were explained using a double resonance process that occurs in single-layer and few layer sheets. We feel that the work presented in this research might be expanded to additional two-dimensional single-layer materials, adding to our understanding of these interesting materials. Temperature dependent Raman spectroscopy can also be applicable for characterizing the optical, electrical, structural, and vibrational properties of additional newly derived single-layer and a few layered Transition metal dichalcogenide materials.

6.2 Future Scope

Photoelectronic devices of MoS_2 are used due to its tunable band gap. However the performance of a device highly depend on thermal conductivity and structural properties of the material, thus we studied Raman Spectroscopy at different temperatures and calculated temperature coefficients for different raman modes comes out to be negative, which tells us that thermal thermal conductivity and electrical resisitivity decreases as temperature increases. Hence due to this property we can use MoS_2 for photoelectronic devices which will not affect by temperature.

References

1. Naumis, G. G. Electronic Properties of Two-Dimensional Materials. In Synthesis, Modeling, and Characterization of 2D Materials, and Their Heterostructures; Elsevier, 2020. https://doi.org/10.1016/B978-0-12-818475-2.00005-2.
2. Late, D. J.; Liu, B.; Matte, H. S. S. R.; Dravid, V. P.; Rao, C. N. R. Hysteresis in SingleLayer MoS_2 Field Effect Transistors. ACS Nano 2012, 6 (6), 5635–5641. https://doi.org/10.1021/nn301572c.
3. Enyashin, A.; Seifert, G. Electronic Properties of MOS_2 Monolayer and Related Structures. Наносистемы: Физика, Химия, Математика 2014, 5 (4).
4. Jayabal, S.; Wu, J.; Chen, J.; Geng, D.; Meng, X. Metallic 1T-MoS_2 Nanosheets and Their Composite Materials : Preparation , Properties and Emerging Applications. Mater. Today Energy 2018, 10, 264–279. https://doi.org/10.1016/j.mtener.2018.10.009.
5. Campos-Roldán, C. A.; Alonso-Vante, N. The Hydrogen Evolution Reaction on Nanostructured Molybdenum Disulfide. J. Mex. Chem. Soc. 2019, 63 (3 Special Issue), 28–38. https://doi.org/10.29356/jmcs.v63i3.533.
6. Wypych, F.; Schollhorn, R. 1T-MoS_2, a New Metallic Modification of Molybdenum Disulfide. No. 1386, 1386–1388.
7. Acerce, M.; Voiry, D.; Chhowalla, M. Metallic 1T Phase MoS_2 Nanosheets as Supercapacitor Electrode Materials. Nat. Nanotechnol. 2015, No. March, 1–6. https://doi.org/10.1038/nnano.2015.40.
8. Kumar, A.; Ahluwalia, P. K. A First Principle Comparative Study of Electronic and Optical Properties of 1H - MoS_2 and 2H - MoS_2. Mater. Chem. Phys. 2012, 135 (2–3), 755–761. https://doi.org/10.1016/j.matchemphys.2012.05.055.
9. Anghel, S.; Chumakov, Y.; Kravtsov, V.; Mitioglu, A.; Plochocka, P.; Sushkevich, K.; Volodina, G.; Colev, A.; Kulyuk, L. Identification of 2H and 3R Polytypes of MoS_2 Layered Crystals Using Photoluminescence Spectroscopy. 2014, 1–7.
10. Arif Khalil, R. M.; Hussain, F.; Manzoor Rana, A.; Imran, M.; Murtaza, G. Comparative Study of Polytype 2H-MoS_2 and 3R-MoS_2 Systems by Employing DFT. Phys. E LowDimensional Syst. Nanostructures 2019, 106, 338–345. https://doi.org/10.1016/j.physe.2018.07.003.

11. Rahman, I. A.; Purqon, A. First Principles Study of Molybdenum Disulfide Electronic Structure. J. Phys. Conf. Ser. 2017, 877 (1). https://doi.org/10.1088/1742-6596/877/1/012026.
12. Tong, X.; Ashalley, E.; Lin, F.; Li, H.; Wang, Z. M. Advances in MoS_2-Based Field Effect Transistors (FETs). Nano-Micro Lett. 2015, 7 (3), 203–218. https://doi.org/10.1007/s40820-015-0034-8.
13. Tsai, M. L.; Su, S. H.; Chang, J. K.; Tsai, D. S.; Chen, C. H.; Wu, C. I.; Li, L. J.; Chen, L. J.; He, J. H. Monolayer MoS_2 Heterojunction Solar Cells. ACS Nano 2014, 8 (8), 8317–8322. https://doi.org/10.1021/nn502776h.
14. Ossila. Molybdenum Disulfide (MoS_2):Theory & Applications https://www.ossila.com/pages/molybdenum-disulfide-mos_2.
15. Kam, K. K.; Parkinson, B. A. Detailed Photocurrent Spectroscopy of the Semiconducting Group VI Transition Metal Dichalcogenides. J. Phys. Chem. 1982, 86 (4), 463–467. https://doi.org/10.1021/j100393a010.
16. Dragoman, M.; Dragoman, D. 2d Nanoelectronics; Springer US, 2017.
17. Behera, A.; Mallick, P.; Mohapatra, S. S. Nanocoatings for Anticorrosion. In Corrosion Protection at the Nanoscale; Elsevier, 2020; pp 227–243. https://doi.org/10.1016/B978- 0-12-819359-4.00013-1.
18. Barua, S.; Geng, X.; Chen, B. Graphene-Based Nanomaterials for Healthcare Applications. In Photonanotechnology for Therapeutics and Imaging; Elsevier, 2020; pp 45–81. https://doi.org/10.1016/B978-0-12-817840-9.00003-5.
19. Madhuri, K. V. Thermal Protection Coatings of Metal Oxide Powders. In Metal Oxide Powder Technologies; Elsevier, 2020; pp 209–231. https://doi.org/10.1016/B978-0-12- 817505-7.00010-5.
20. Novoselov, K. S., & Castro Neto, A. H. (2012). Two-dimensional crystals-based heterostructures: Materials with tailored properties. Physica Scripta, T146. https://doi.org/10.1088/0031-8949/2012/T146/014006.
21. Sun, J., Li, X., Guo, W., Zhao, M., Fan, X., Dong, Y., Xu, C., Deng, J., & Fu, Y. (2017). Synthesis methods of two-dimensional MoS_2: A brief review. Crystals, 7(7), 1–11. https://doi.org/10.3390/cryst7070198.
22. Humphreys, C. J. (2013). The significance of Braggs law in electron diffraction and microscopy, and Braggs second law. Acta Crystallographica Section A: Foundations of Crystallography, 69(1), 45–50. https://doi.org/10.1107/S0108767312047587.

23. Temperature Dependent Phonon Shifts in Single-Layer WS_2 . Thripuranthaka M. and Dattatray J., Late , dx.doi.org/10.1021/am404847d.
24. Temperature dependent Raman spectroscopy of chemically derived few layer MoS_2 and WS_2 nanosheets. http://dx.doi.org/10.1063/1.4866782.
25. Anharmonicity of monolayer MoS2, MoSe2, and WSe2: A Raman study under high pressure and elevated temperature. http://dx.doi.org/10.1063/1.4977877.
26. Resonance Raman scattering in bulk 2H-MX_2 (M=Mo, W; X=S, Se) and monolayer MoS_2 Jia-He Fan, Po Gao, An-Min Zhang, Bai-Ren Zhu, Hua-Ling Zeng, Xiao-Dong Cui, Rui He, and Qing-Ming Zhang.
27. Quantitative Analysis of Temperature Dependence of Raman shift of monolayer WS_2. DOI: 10.1038/srep32236.
28. Bhattacharya, D., Mukherjee, S., Mitra, R. K., & Ray, S. K. (2000). Size dependent optical properties of MoS_2 nanoparticles and their photo-catalytic applications.
29. Blodgett, K. B. (1935). Films Built by Depositing Successive Monomolecular Layers on a Solid Surface. Journal of the American Chemical Society, 57(6), 1007–1022. https://doi.org/10.1021/ja01309a011.
30. Wang, H., Li, C., Fang, P., Zhang, Z., & Zhang, J. Z. (2018). Synthesis, properties, and optoelectronic applications of two-dimensional MoS2 and MoS2-based heterostructures. Chemical Society Reviews, 47(16), 6101–6127. https://doi.org/10.1039/c8cs00314a.
31. Windom, B. C., Sawyer, W. G., & Hahn, D. W. (2011). A raman spectroscopic study of MoS 2 and MoO 3: Applications to tribological systems. Tribology Letters, 42(3), 301–310. https://doi.org/10.1007/s11249-011-9774-x.
32. Withanage, S. S., Kalita, H., Chung, H. S., Roy, T., Jung, Y., & Khondaker, S. I. (2018). Uniform Vapor-Pressure-Based Chemical Vapor Deposition Growth of MoS2 Using MoO3 Thin Film as a Precursor for Coevaporation [Research-article]. ACS Omega, 3(12), 18943–18949. https://doi.org/10.1021/acsomega.8b02978.
33. Yale University. (n.d.). West Campus Materials Characterization Core. Retrieved June 03, 2020, from https://ywcmatsci.yale.edu/: https://ywcmatsci.yale.edu/xps.
34. Campbell, B.; Manning, J. The Rise of Victimhood Culture: Microaggressions, Safe Spaces, and the New Culture Wars. Rise Vict. Cult. Microaggressions, Safe Spaces, New Cult. Wars 2018, 1–265. https://doi.org/10.1007/978-3-319-70329-9.

35. Ma, D.; Shi, J.; Ji, Q.; Chen, K.; Yin, J.; Lin, Y.; Zhang, Y.; Liu, M.; Feng, Q.; Song, X.; Guo, X.; Zhang, J.; Zhang, Y.; Liu, Z. A Universal Etching-Free Transfer of MoS2 Films for Applications in Photodetectors. Nano Res. 2015, 8 (11), 3662–3672. https://doi.org/10.1007/s12274-015-0866-z.
36. TWI. What is X-Ray diffraction analysis (XRD) and how does it work? https://www.twi-global.com/technical-knowledge/faqs/x-ray-diffraction.
37. Dutrow, B.; Lousiana State University; Clark, C.; Estern Michigan University. X-Ray Powder Diffraction.
38. Thermo scientific XPS. What is X-ray Photoelectron Spectroscopy (XPS)? https://xpssimplified.com/whatisxps.php.
39. Woods, J.; CHEMISTRY LibreTexts. Photoelectron Spectroscop:Application https://chem.libretexts.org/Bookshelves/Physical_and_Theoretical_Chemistry_Textbook_Maps/Supplemental_Modules_(Physical_and_Theoretical_Chemistry)/Spectroscop y/Photoelectron_Spectroscopy/Photoelectron_Spectroscopy%3A_Application.
40. Campos-Roldán, C. A.; Alonso-Vante, N. The Hydrogen Evolution Reaction on Nanostructured Molybdenum Disulfide. J. Mex. Chem. Soc. 2019, 63 (3 Special Issue), 28–38. https://doi.org/10.29356/jmcs.v63i3.533.
41. Thermo Fisher Scientific Phenom World-BV. (2018, April 4). News Medical LIfe Sciences. Retrieved June 01, 2020, from www.news-medical.net: https://www.newsmedical.net/whitepaper/20180404/Studying-Blood-Disorders-with-SEM-andCLEM.asp.
42. The University of Texas at Austin - Centre for Space Research. (2019). Hyperspectral Remote Sensing. Retrieved July 24, 2019, from Centre for Space Research: http://www.csr.utexas.edu/projects/rs/hrs/hyper.html.
43. Shippert, P. (April 2004). Why Use Hyperspectral Imagery? PHOTOGRAMMETRIC ENGINEERING & REMOTE SENSING, 377-380.
44. NASA Jet Propulsion Laboratory / California Institute of Technology. (2019). New Millennium Program. Retrieved July 24, 2019, from NASA Jet Propulsion Laboratory / California Institute of Technology: https://www.jpl.nasa.gov/nmp/PROGRAM/programindex.php.
45. Mishra, D. (2010). New algorithm development for snow cover monitoring at sub-pixel level. Atti Della Fondazione Giorgio Ronchi Fondata Da Ronchi, 439.